ELSEVIER

Hearing Research 174 (2002) 206–221

HEARING RESEARCH

www.elsevier.com/locate/heares

Tuning and timing in the gerbil ear: Wiener-kernel analysis

Edwin R. Lewis [a,*], Kenneth R. Henry [b], Walter M. Yamada [c]

[a] *Department of Electrical Engineering and Computer Science, University of California, Berkeley, CA 94720, USA*
[b] *Department of Psychology, University of California, Davis, CA 95616, USA*
[c] *Biomedical Simulations Resource, University of Southern California, Los Angeles, CA 90089, USA*

Received 4 March 2002; accepted 3 September 2002

Abstract

Information about the tuning and timing of excitation in cochlear axons with low-characteristic frequency (CF) is embodied in the first-order Wiener kernel, or reverse correlation function. For high-CF axons, the highest-ranking eigenvector (or singular vector) of the second-order Wiener kernel often can serve as a surrogate for the first-order kernel, providing the same information. For mid-CF axons, the two functions are essentially identical. In this paper we apply these tools to gerbil cochlear-nerve axons with CFs ranging from 700 Hz to 14 kHz. Eigen or singular-value decomposition of the second-order Wiener kernel allows us to separate excitatory and suppressive effects, and to determine precisely the timing of the latter.

Key words: Tuning; Temporal response; Suppression; Reverse correlation; Gerbil cochlea

1. Introduction

In a previous paper (Lewis et al., 2002)) we demonstrated that simple matrix manipulation allows one to decompose the second-order Wiener kernel into two subkernels, one representing excitatory processes, the other inhibitory or suppressive processes. The decomposition also allows us to give simple physiological interpretation to the subkernels and their vector elements. In that paper, we applied the analysis to afferent axons of the frog's principal auditory sensor, the amphibian papilla. In this paper, we apply it to afferent axons of the gerbil cochlear nerve.

2. Methods

The analytical methods used for this paper are the same as those described in Lewis et al. (2002). All of the first-order Wiener kernels computed in this paper are 400-element vectors; and all of the second-order kernels are 400×400 matrices. Axonal recordings were made intracellularly, with glass micropipettes, on anesthetized Mongolian gerbils (*Meriones unguiculatus*) with temperatures maintained within 1°C of normal. All animals were free of aural cholesteatoma and had compound action potential (CAP) thresholds at 8 kHz that remained below 20 dB SPL throughout the experiment. Noise stimuli were presented in closed-field configuration through an Etymotic ER-2 driver. They were observed through a calibrated microphone (Etymotic ER-10B) sealed to the external ear canal. The output of the microphone was applied to a Hewlett-Packard 3561A Dynamic Signal Analyzer, and its spectral content was observed continuously through each experiment. Prior to being applied to the driver, the stimulus signal was passed through a parametric equalizer (Rane PE-15) followed by two third-octave graphic equalizers (Rane GQ-30). With a spectrally flat input to the parametric equalizer, from a General Radio Gaussian White Noise

* Corresponding author. Tel.: +1 (510) 642 5169; Fax: +1 (510) 643 8426.
E-mail address: lewis@eecs.berkeley.edu (E.R. Lewis).

Abbreviations: ac, alternating current; CAP, compound action potential; CF, characteristic frequency; dc, direct current; DFT, discrete Fourier transform; exc, excitatory; FTC, frequency–threshold tuning curve; inh, inhibitory; PSTH, peristimulus time histogram; REVCOR, reverse correlation; SV, singular vector

0378-5955/02/$ – see front matter
PII: S0378-5955(02)00695-0

Generator (Model 1390-B), all three equalizers were adjusted to make the noise measured in the ear canal spectrally flat (±3 dB) from 300 Hz to 17 kHz. Electrode- and stimulus-waveform recordings were digitized (40-kHz sampling rate for axons with low-characteristic frequency (CF), 80-kHz for high-CF axons), and for each spike the sampling interval during which it passed through its peak was estimated and taken to be the moment of its occurrence. Detailed descriptions of animal maintenance, anesthesia, surgery, and recording techniques are given in earlier papers (e.g., see Lewis and Henry, 1995)[1].

3. First-order Wiener kernels

3.1. Background

Cochlear axons with low CFs typically exhibit strong phase locking at frequencies that include CF. For such axons, the first-order Wiener kernel, sometimes called the reverse correlation (REVCOR) function (de Boer and Kuyper, 1968), has proved to be an excellent predictor of peristimulus time histograms (PSTHs) in response to repeated novel stimulus waveforms (de Boer and de Jongh, 1978; Carney and Yin, 1988; Wolodkin et al., 1997). The stimulus waveforms can be of arbitrary complexity, but they must be presented either with nearly 100% duty cycle or in the presence of background sound of approximately the same power density level. Thus, under conditions of constant or nearly constant sound level, the first-order Wiener kernels appear to represent very well the signal-processing properties of low-CF cochlear axons, including the spectrotemporal properties of the cochlear tuning structures associated with them. Discrete Fourier transforms (DFTs) of these Wiener kernels typically yield amplitude tuning curves with approximately 20 dB of dynamic range exposed above the noise floor. Over that 20-dB range, they consistently match the tuning curves (FTCs) derived by plotting threshold vs. frequency (Evans, 1989).

3.2. Results from the gerbil

The left-hand column of Fig. 1 shows first-order Wiener kernels (REVCOR functions) measured for five low-CF axons from the gerbil. These were selected (from several hundred axons) to represent the frequency range from 700 Hz (top) to 2.8 kHz (bottom) in steps of approximately 0.5 octave. The amplitude portions of the DFTs of these kernels are shown in the corresponding panels in Fig. 2. From top to bottom in the left-hand column, the noise stimulus levels used to obtain the kernels (in dB SPL, observed for a 100-Hz bandwidth at 8kHz) were 36, 34, 37, 37 and 28. Fig. 3 shows another first-order Wiener kernel (taken at 31 dB SPL for 100 Hz bandwidth at 8 kHz) for the axon of the bottom left-hand panels of Figs. 1 and 2, along with its prediction of the PSTH that axon should produce in response to a specific complex waveform at approximately the same intensity level. The prediction was constructed by convolution of the kernel with the stimulus waveform:

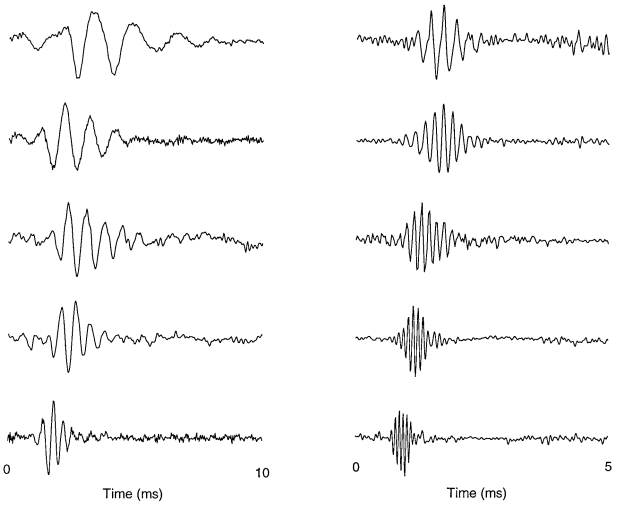

Fig. 1. Filter functions for 10 gerbil cochlear-nerve axons, with CFs at approximately half-octave intervals. The filter functions on the left (CFs ranging from 700 Hz to 2.8 kHz, top to bottom) are first-order Wiener kernels, estimated by first-order REVCOR between times of spike occurrences and a continuing white-noise stimulus. The filter functions on the right (CFs ranging from 4 kHz to 14 kHz, top to bottom) are the highest-ranking singular vectors (eigenvectors in this case) of second-order Wiener kernels. The kernels in that case were estimated by second-order REVCOR between spike times and the noise stimulus. Notice that the waveforms on the left all span 10 ms; those on the right all span 5 ms. Notice as well that the tuned portion of the waveform for the 14-kHz axon falls within less than 1 ms.

$$r_1(n) = \sum_{\tau=0}^{N=1} h_1(\tau)s(n-\tau) \quad (1)$$

where $r_1(n)$ is the content of the nth bin of the response histogram (PSTH); $h_1(\tau)$ is the REVCOR function (first-order Wiener kernel), τ being time and N being the number of elements (sampling intervals) in the discrete function, $h_1(\tau)$; $s(\tau)$ is the stimulus waveform.

The stimulus waveform was a randomly selected segment of band-limited white noise. It had a duration of approximately 74 ms, with 1.0 ms rise time at its onset, and 1.0 ms fall time at its termination. It was repeated approximately 2400 times with no time gap between the

[1] All animal experiments were performed in accordance with protocols approved by the Animal Care and Use Committees at UC Davis and UC Berkeley (protocols #6797 and R081-1097, respectively).

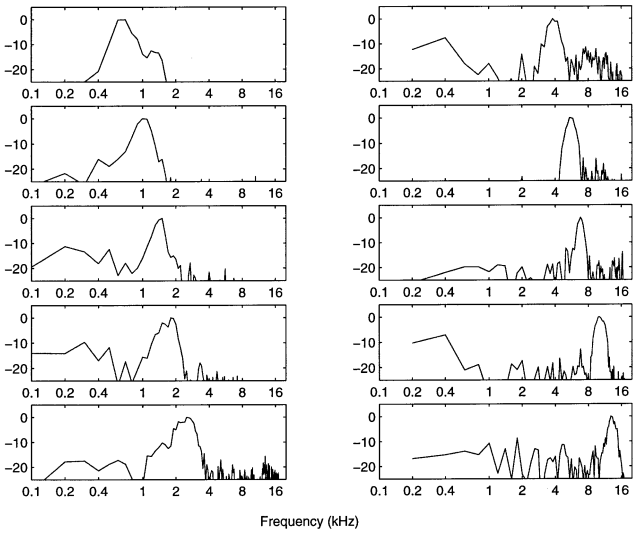

Fig. 2. Amplitude portions of the DFTs of the waveforms in Fig. 1. The vertical scale is given in decibels (re the peak amplitude of the tuning curve). All 10 curves are plotted over the same frequency range.

termination of one presentation and onset of the subsequent presentation. To avoid edge effects in the convolution computation, $s(\tau)$ in Eq. 1 comprised the last 10 ms of the 74-ms segment followed by the entire segment (beginning with its onset). The second panel of Fig. 3 shows the predicted and observed PSTHs beginning at the onset of the segment. For comparison, the amplitudes of the predicted and observed PSTHs both were normalized. For the observed PSTH, the normalization factor was the rms value of the entire waveform; for the predicted PSTH, it was half the rms value of the entire waveform.

The precision of correspondence between the predicted and observed phase is remarkable. In general, we find that such precision requires that the first-order kernel be taken in close temporal proximity to the taking of the PSTH. In this axon, for example, the waveform in the lower right of Fig. 1 (taken 20 min earlier) produced a prediction with slight, but noticeable phase error. With the REVCOR function of Fig. 3, which was taken immediately after the prediction run, the phase prediction was accurate to within the resolution of the histogram (0.0125 ms). Although there is some slow drift in the baseline of the prediction, the cycle-by-cycle amplitudes of its positive excursions match very well those of the observed PSTH. The results in Fig. 3 are typical of what we have found in the gerbil cochlea and the frog amphibian papilla (Wolodkin et al., 1996; Yamada, 1997). Thus, just as de Boer and de Jongh (1978) concluded more than 20 years ago, we conclude that the first-order Wiener kernel (REVCOR function) represents with considerable fidelity important aspects of current dynamics of the low-CF auditory axon.

One must realize that there are important constraints on this fidelity. One of these, obvious in Fig. 3, is the prediction of negative excursions of instantaneous spike rate. These, of course, will be seen in the observed PSTH only if they are superimposed on sufficient background spike activity (see Lewis and Henry, 1995). If the background activity is not sufficient, the negative excursions will be clipped at zero spikes/s in the observed PSTH – as they were in Fig. 3. Another constraint is the amplitude specificity of the Wiener kernel. The shape and amplitude of the function changes as the amplitude of the noise stimulus used to derive it is changed (Evans, 1977; Møller, 1986; Carney and Yin, 1988; Lewis and Henry, 1994). These amplitude and

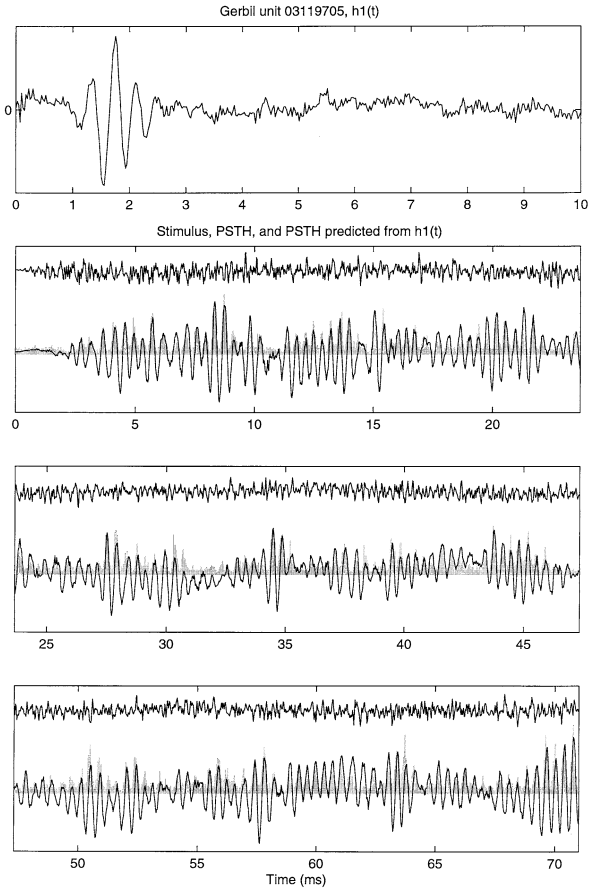

Fig. 3. (Top panel) First-order kernel (filter function) for the axon of the bottom-left panels in Figs. 1 and 2, taken approximately 20 min after that in Fig. 1. (Lower three panels) The top line in each panel shows a segment of a repeated stimulus waveform, recorded with a calibrated probe microphone (Etymotic ER-10B) tightly sealed to the animal's ear canal. The corresponding PSTH of spike-time distributions is shown in gray. The PSTH is based on 19 412 spikes obtained from 2370 repetitions of the stimulus waveform. The black line superimposed upon the PSTH is a prediction of it, derived from convolution of the filter function in the top panel with the stimulus waveform. Thus, for this prediction, the filter is taken to be linear, with its filter function being the waveform in the top panel. The instantaneous spike-rate response clearly is tightly phase-locked to the filtered waveform.

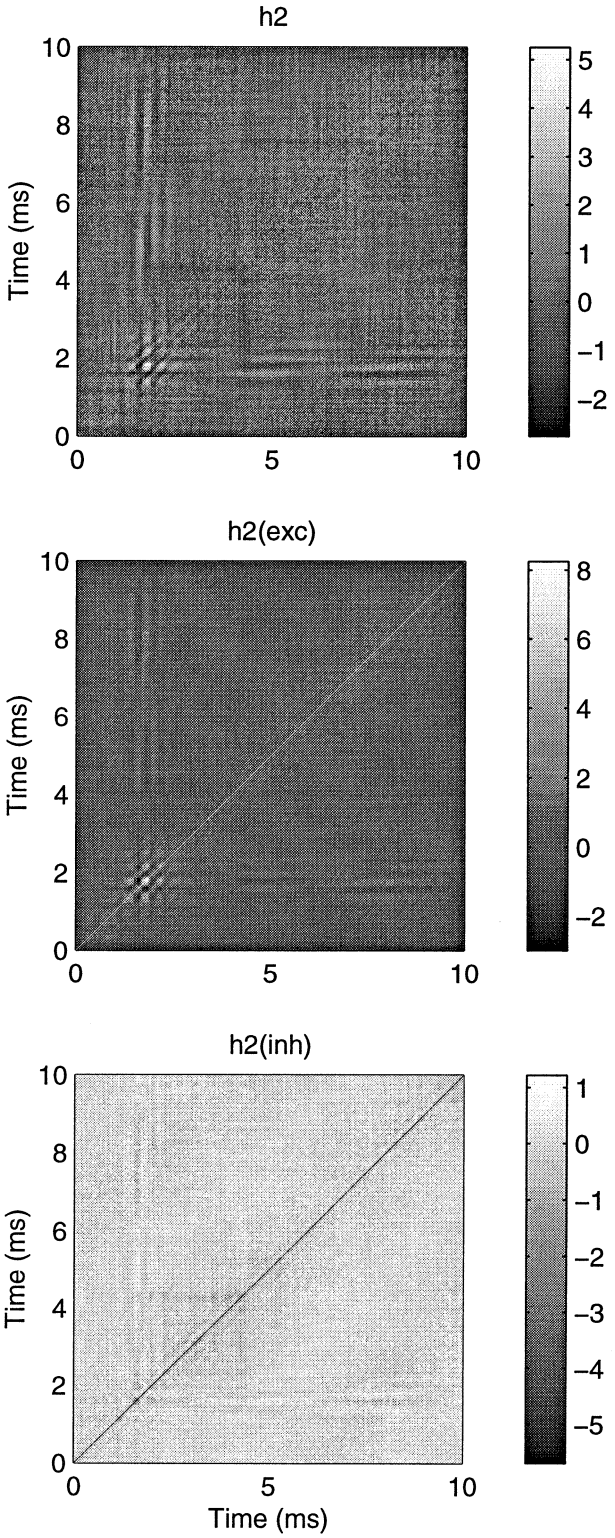

Fig. 4. (Top) Second-order Wiener kernel (h2) for the axon of Fig. 3 (CF = 2.8 kHz). (Middle and bottom) Excitatory and inhibitory subkernels, respectively, of h2. The checkerboard patterns in these kernels represent second-order (square-law) distortion to be added (h2exc) to, or subtracted (h2inh) from, the prediction from the first-order Wiener kernel. Among other things, it will provide an approximation to the clipping of the PSTH at zero spikes/s.

shape changes reflect changes in gain and tuning. The impact of these changes is especially evident in PSTHs generated with stimulus waveforms presented with low duty cycles – i.e., with the offset of each presentation of the stimulus waveform separated from the onset of the subsequent presentation by a substantial silent period. When we have done this with low-spontaneous-rate gerbil axons, for example, the amplitudes of the phase-locked excursions in the early parts of the predicted PSTHs are conspicuously (e.g., 10-fold) lower than those of the observed PSTHs. The predictions also exhibit phase errors. Predictions for the later portions of the PSTH, however, are comparably faithful to those in Fig. 3. Specific results will be presented in a subsequent paper.

Eq. 1 describes the second term of the Wiener series:

$$r(n) = h_0 + \sum_{\tau=0}^{N-1} h_1(\tau)s(n-\tau) + \sum_{\tau=0}^{N-1}\sum_{\tau=0}^{N-1} h_2(\tau_1,\tau_2)s(n-\tau_1)$$
$$s(n-\tau_2) + \ldots = r_0 + r_1(n) + r_2(n) + \ldots \quad (2)$$

where the kernel, $h_2(\tau_1,\tau_2)$, of the third term in the series is an $N\times N$ array of real numbers. This kernel (the second-order Wiener kernel) was introduced previously to the hearing research community by Eggermont et al. (1983c) (see also Eggermont et al., 1983a,b; Eggermont, 1993), and van Dijk et al. (1994, 1997a,b). Among the first three terms of the series (0th order, 1st order and 2nd order), it is only the third that begins to contribute to prediction of clipping at zero spikes/s. In our previous paper (Lewis et al., 2002), we demonstrated that it also bears implications regarding direct current (dc) (envelope-following) responses as well as forms of adaptation and suppression. In the remainder of this paper, we

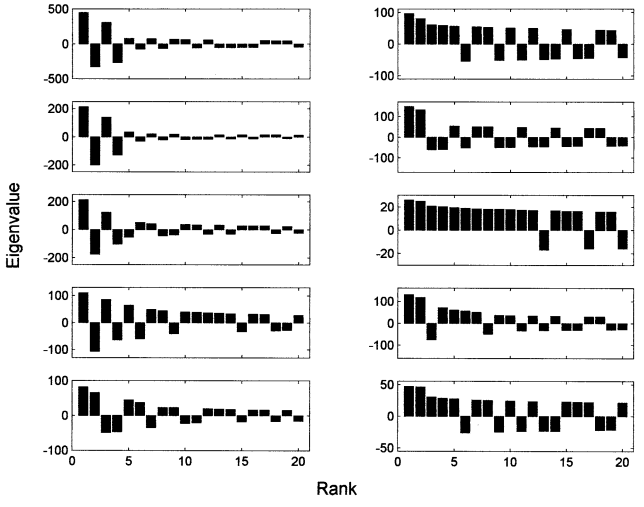

Fig. 5. Highest-ranking eigenvalues of the second-order Wiener kernels for the axons of Figs. 1 and 2, presented in the same spatial order.

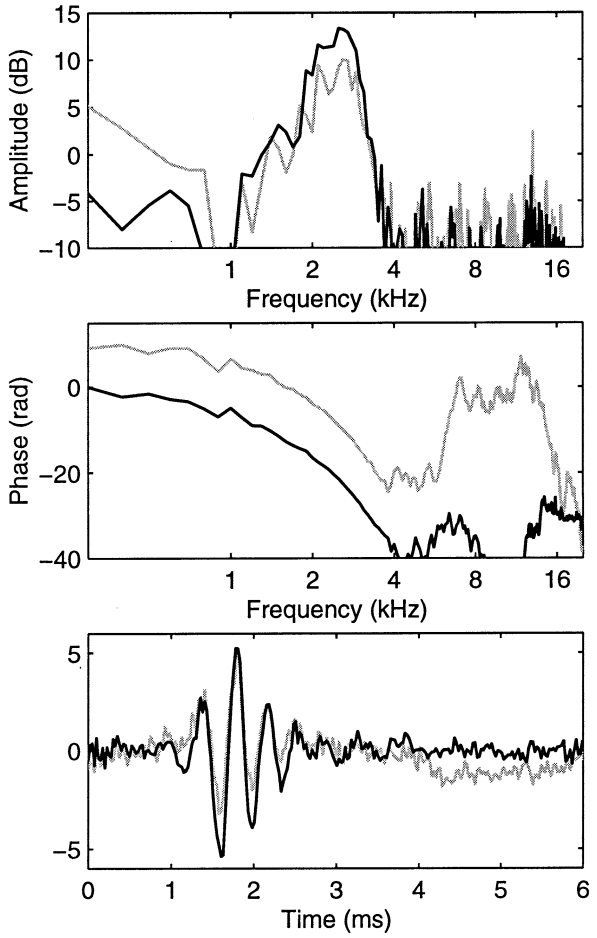

Fig. 6. Comparison of the first-order Wiener kernel (black line) and the highest-ranking (rank-1) eigenvector (gray line) of the second-order kernel for the axon of Fig. 3 (bottom left panels in Figs. 1, 2 and 5). The temporal waveforms (filter functions), shown in the bottom panel, have been normalized in amplitude for comparison of shape. Above them are shown the phase and amplitude portions of their DFTs. Notice the near-perfect match between the waveforms, which is typical for mid- to high-frequency axons.

shall examine the second-order Wiener kernels of several gerbil cochlear-nerve axons, along with some implications from these kernels.

4. Second-order Wiener kernels

4.1. Background

The second-order Wiener kernel is derived from second-order REVCOR between spikes and a continuous, nonrepeating, broadband white-noise stimulus. Because the stimulus waveform is digitized, the kernel takes the form of a two-dimensional array (matrix) of real numbers. By the way in which it is constructed, the matrix is square and symmetric about its main diagonal axis. By

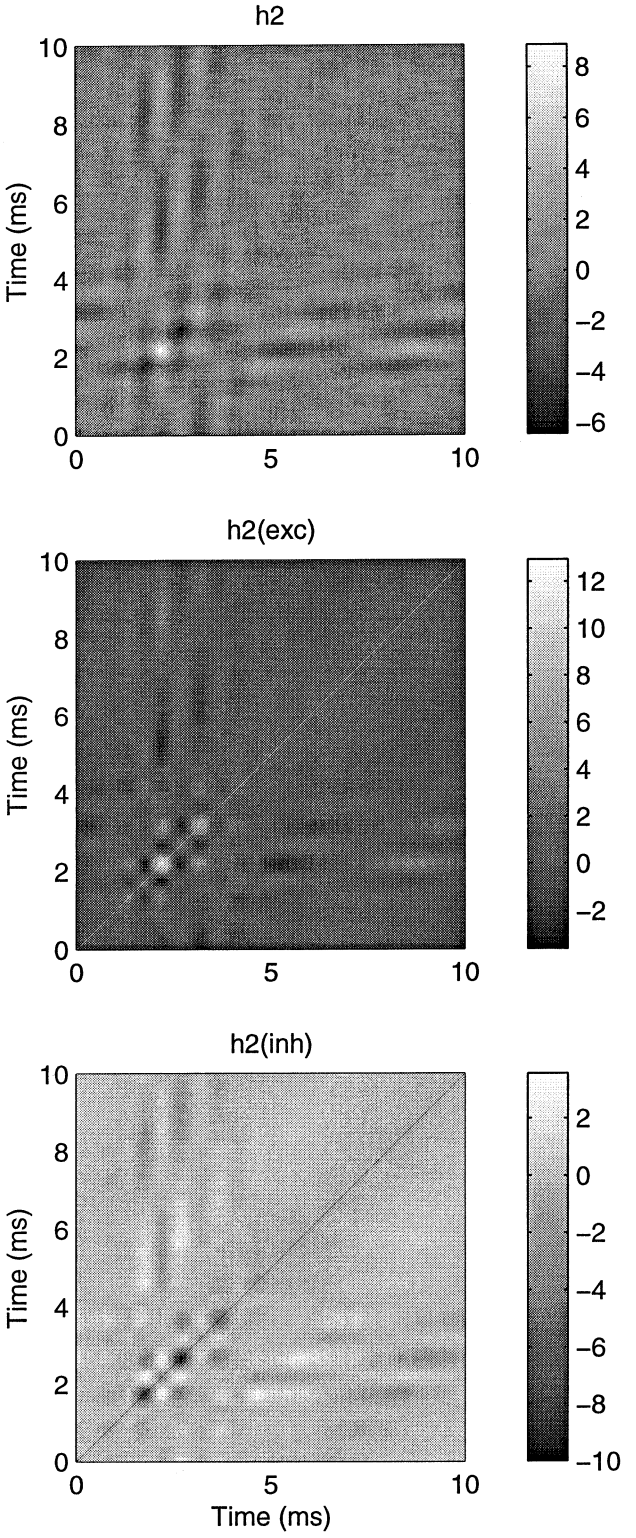

Fig. 7. (Top) Second-order Wiener kernel (h2) for the axon of the second panel from the top in the left column of Figs. 1, 2 and 5 (CF = 1.0 kHz). (Middle and bottom) Excitatory and inhibitory subkernels, respectively, of this h2. The patterns in these three panels are fairly typical of second-order kernels for low-frequency gerbil axons. Again, the checkerboarding reflects second-order distortion of the predicted PSTH.

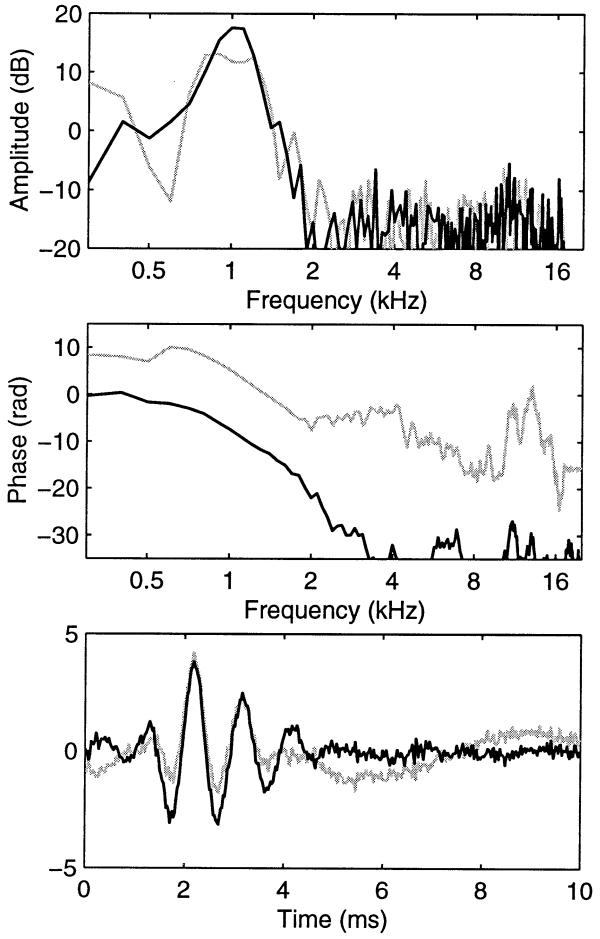

Fig. 8. Comparison of the first-order Wiener kernel (black line) and the highest-ranking (rank-1) eigenvector (gray line) of the second-order kernel for the axon of Fig. 7. Again, the amplitudes have been normalized. The match between the waveforms, typical of low-frequency gerbil axons, is not quite as good as that for mid- to high-frequency axons.

the process of singular-value decomposition (or, equivalently for symmetric, square matrices with real elements, by eigenvector decomposition) the kernel can be decomposed into two subkernels – one reflecting processes that lead to increases in instantaneous spike rate, the other reflecting processes that lead to decreases in instantaneous spike rate (Lewis et al., 2002). For low- to mid-frequency axons, the second-order kernels and subkernels typically include checkerboard patterns. For all axons they may include patterns of parallel diagonal lines. The checkerboard patterns represent nonlinearities in the phase-locked (alternating current (ac)) response of the axon; the diagonal lines reflect nonlinear envelope-following (dc) responses. Detailed interpretation of these patterns in terms of time and frequency is aided by studying the highest-ranking eigenvectors (singular vectors) and their DFTs (Yamada, 1997; Yamada and Lewis, 1999; Lewis et al., 2002).

4.2. Results from the gerbil

Fig. 4 shows a 400×400 second-order Wiener kernel (along with its excitatory (exc) and inhibitory (inh) subkernels) for the axon of Fig. 3. The element-by-element sum of the two subkernels, h2(exc) and h2(inh), equals the complete kernel, h2. Fig. 5 shows the 20 highest-ranking eigenvalues of the second-order Wiener kernels for the axons of Figs. 1 and 2. In each panel, the positive eigenvalues correspond to eigenvectors from the excitatory subkernel and the negative eigenvalues correspond to eigenvectors from the inhibitory subkernel (see Lewis et al., 2002). These second-order kernels were computed from the same data that were used to compute the first-order kernels of Fig. 1. The eigenvalues for the axon of Fig. 3 are displayed in the bottom panel of the left column of Fig. 5. The bottom panel of Fig. 6 shows the highest-ranking (rank-1) eigenvector for the axon of Fig. 3, along with the first-order Wiener kernel. The fact that these two waveforms have essentially the

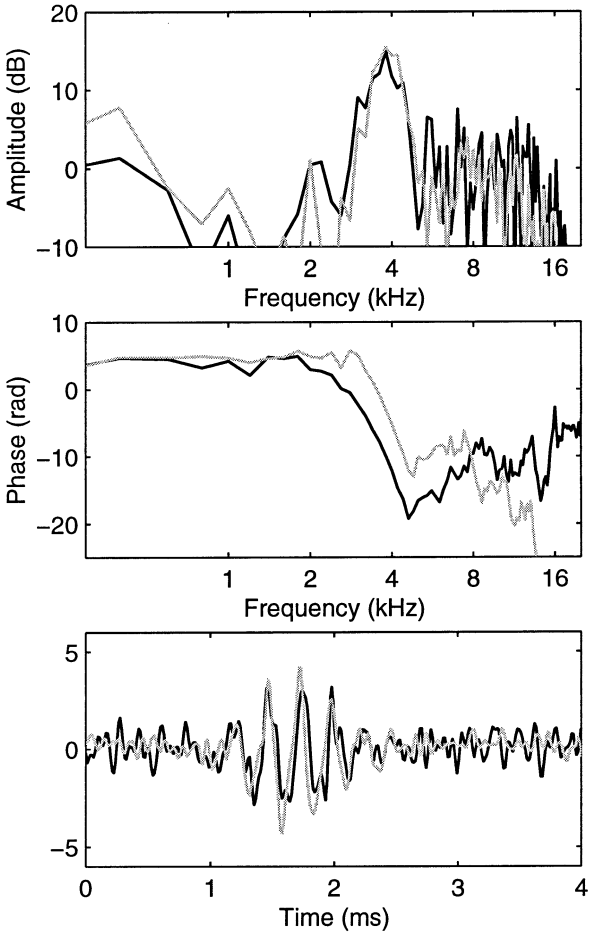

Fig. 9. Comparison of the first-order Wiener kernel (black line) and the highest-ranking (rank-1) eigenvector (gray line) of the second-order kernel for the axon of the top right panel in Figs. 1, 2 and 5. The match between the amplitude-normalized waveforms again is near perfect.

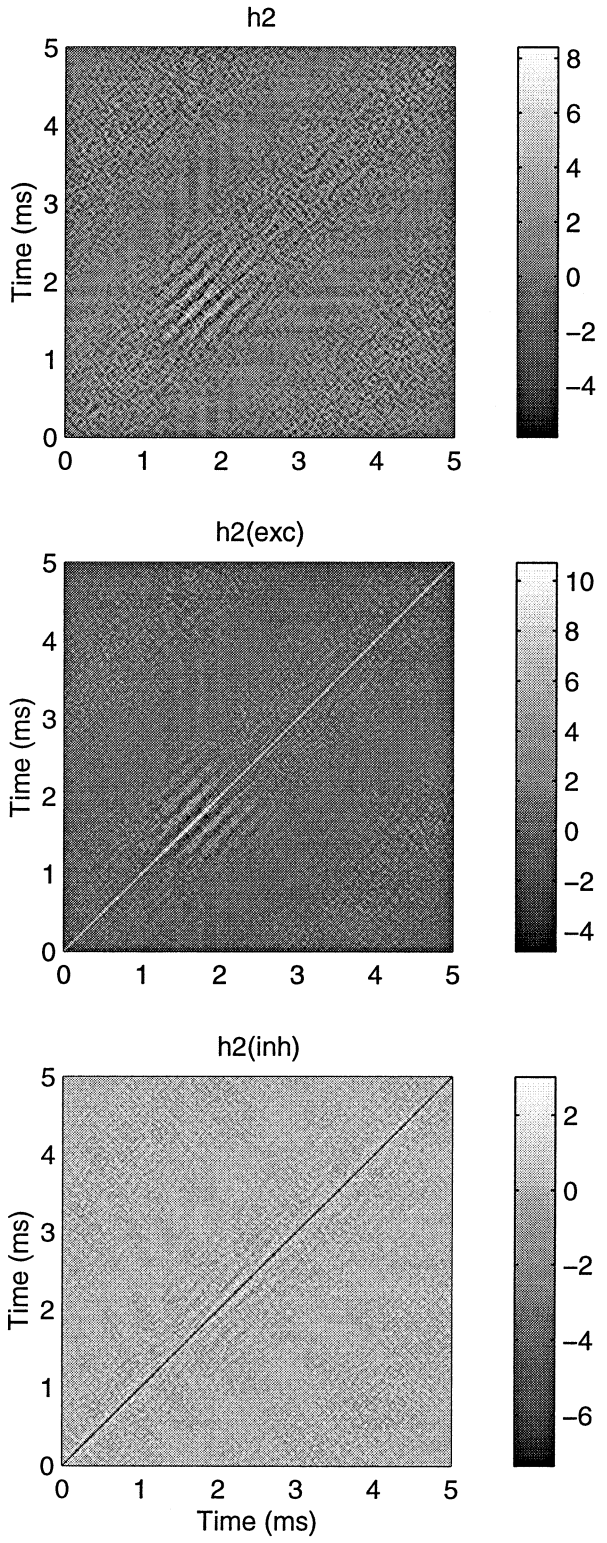

Fig. 10. Second-order Wiener kernel, with excitatory and inhibitory subkernels, for the axon of Fig. 9. Notice the apparent lack of checkerboard pattern. The pattern of parallel diagonal lines represents a PSTH component that is phase-locked to the square of the envelope of a filtered version of the stimulus waveform. The filter function would be the waveform of Fig. 9. If the stimulus waveform were a constant-amplitude sine wave, the response predicted by this h2 would be a positive constant (dc) spike rate.

same shape implies that we are dealing with a single peripheral tuning structure, whose impulse response also has the same shape (Lewis et al., 2002). The dominant pattern in the second-order kernel of Fig. 4 (in the vicinity of 2 ms) has both parallel diagonal lines and checkerboard elements.

In light of the DFT in Fig. 6, one can interpret these observations as follows (see Lewis et al., 2002). At the present moment (represented by the origin in Fig. 4), the instantaneous spike rate of this axon will have a component that is phase-locked to a filtered version of any stimulus waveform that occurred between approximately 1 and 3 ms ago and contained spectral energy in the neighborhood of 2.8 kHz. That phase-locked component will include a linear subcomponent (implied by the first-order Wiener kernel) and a second-harmonic (square-law) distortion subcomponent (implied by the checkerboard pattern in the vicinity of 2 ms in the second-order kernel). At the present moment, the instantaneous spike rate will also have a component that is phase-locked to the square of the positive envelope of the same filtered waveform (implied by the parallel diagonal lines in the vicinity of 2 ms in the second-order kernel). The impulse response and tuning of the filter in question are given by graphs in Fig. 6.

Fig. 7 shows the second-order Wiener kernel for the axon of the second panel from the top in the left columns of Figs. 1 and 2. The patterns in the kernel and the flip-flopping distribution of highest-ranking positive and negative eigenvalues (second panel from top of left column in Fig. 5) are typical of low-CF gerbil axons, and representative of the four lowest-CF axons of Figs. 1, 2 and 5. The closeness of the match between the first-order Wiener kernel and the highest-ranking eigenvector (Fig. 8) again suggest a single peripheral tuning structure. The imperfection in the match in the interval between 4 and 5 ms is a consequence of the fact that the tuning structure was represented in part by this eigenvector and in part by the second-ranking eigenvector – a common observation for low-CF gerbil axons (see Appendix of Lewis et al., 2002). Taken together, the first- and second-order kernels in this case imply that the present instantaneous spike rate will have a response component phase-locked to a filtered version of any stimulus waveform that occurred between 1 and 5 ms ago and contained spectral energy in the vicinity of 1 kHz. Again, there will be a linear subcomponent and a second-harmonic distortion subcomponent.

Fig. 9 shows the first-order Wiener kernel and the highest-ranking (excitatory) eigenvector of the second-order kernel (Fig. 10) for the 4-kHz axon of Figs. 1, 2 and 5. The closeness of the match implies that, once again, we are dealing with a single peripheral tuning structure, whose impulse response is given by either waveform in the bottom panel of Fig. 9. The dominant

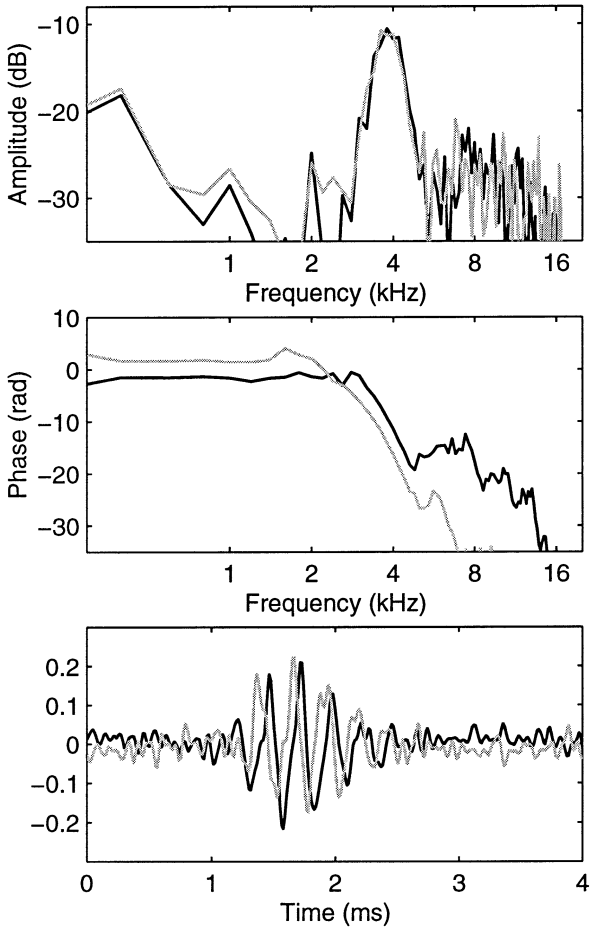

Fig. 11. Comparison of the two highest-ranking eigenvectors of the second-order kernel of Fig. 10. The rank-1 eigenvector (SV1) and its DFT are shown in black, the rank-2 eigenvector (SV2) and its DFT in gray. These two vectors form a quadrature pair and are responsible in large measure for the parallel diagonal lines in the excitatory subkernel in Fig. 10 (see Fig. 12).

pattern in the second-order kernel (top panel of Fig. 10) is a distinct patch comprising alternately light and dark, parallel diagonal lines. Any checkerboarding in this patch is weak. Decomposition shows that this pattern resides almost entirely in the excitatory subkernel (middle panel of Fig. 10). These features are typical of all gerbil axons with CFs higher than 4 kHz. For all such axons, this implies that the predominant contribution of the second-order kernel to a predicted PSTH will be an excitatory component (an increase in instantaneous spike rate) that is phase-locked to the square of the positive envelope of a filtered version of the stimulus waveform (Lewis et al., 2002). The presence of the well-tuned first-order kernel for this 4-kHz axon, however, implies that for this axon there also was a significant response component phase-locked to the filtered waveform itself (as opposed to the square of its positive envelope).

After eigen decomposition, a pattern of parallel, di-

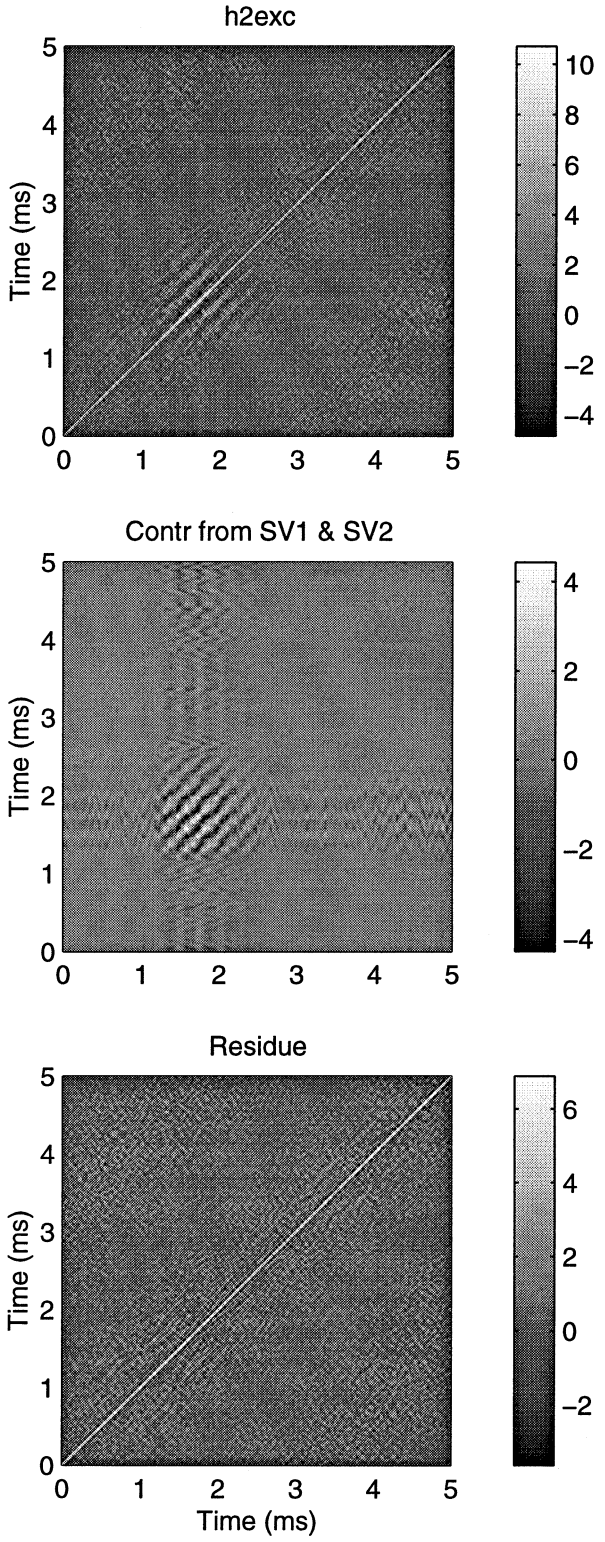

Fig. 12. Decomposition of the excitatory subkernel (h2exc) of Fig. 10. The middle panel shows the contribution from the quadrature pair of eigenvectors (SV1 and SV2) of Fig. 11. The bottom panel shows the contribution from the remaining excitatory eigenvectors. The matrix (h2exc) in the top panel equals the sum of the other two matrices.

agonal lines centered about the main diagonal (i.e., the rising diagonal in the second-order kernels shown in this paper) is represented by one or more quadrature pairs of eigenvectors, such as those shown in the bottom panel of Fig. 11. One member of each quadrature pair has essentially the same shape as the other, but it is phase-shifted by one-quarter cycle (see Yamada and Lewis, 1999; Lewis et al., 2002). The quadrature pair in Fig. 11 comprises the two highest-ranking eigenvectors, SV1 and SV2 (singular vectors of ranks 1 and 2), of the second-order Wiener kernel of Fig. 10. From the top panel of Fig. 5, one can see that both of these eigenvectors have positive eigenvalues. That means that both contribute to the excitatory subkernel, h_2(exc) in Fig. 10. In the middle panel of Fig. 12, we have reconstructed that contribution. The bottom panel in Fig. 12 shows the remainder of h2(exc) after the contribution from SV1 and SV2 have been subtracted (the matrix in the top panel is the sum of the two matrices below it).

It is clear that the two eigenvectors of Fig. 11 are almost entirely responsible for the pattern of parallel diagonal lines in h2(exc). Thus they can be taken together to embody response dynamics represented by that pattern. Furthermore, because one of them matches so well the first-order kernel for the axon (Fig. 9), this highest-ranking quadrature pair (and its DFTs) can be taken to be faithful surrogates for the first-order kernel (REVCOR function). Therefore, in Figs. 1 and 2 (top panel, right column), we represented this axon by the highest-ranking eigenvector of its second-order Wiener kernel, rather than by its first-order Wiener kernel. For the remaining axons of the right columns of Figs. 1, 2 and 5, the first-order Wiener kernels exhibited no tuning, owing to the fact that CFs were well above the highest frequencies at which significant phase locking occurs. In each case, the highest-ranking eigenvectors (ranks 1 and 2) had positive eigenvalues and formed a quadrature pair. Furthermore, in each case those two eigenvectors were the only ones that had both positive eigenvalues and conspicuous tuning; and in each case those two eigenvectors accounted for almost the entire pattern of parallel diagonal lines in the excitatory subkernel. Therefore, although there were no tuned first-order kernels with which to compare them, the highest-ranking members of those quadrature pairs were presented in the right columns of Figs. 2 and 3 to represent the tuning properties of the axons. From top to bottom in the right-hand column of Figs. 1, 2 and 5, the noise intensity levels used to obtain the second-order kernels (in dB SPL for 100-Hz bandwidth at 8 kHz) were 25, 27, 35, 36 and 35.

4.3. Suppression

Among the five axons represented in the right col-

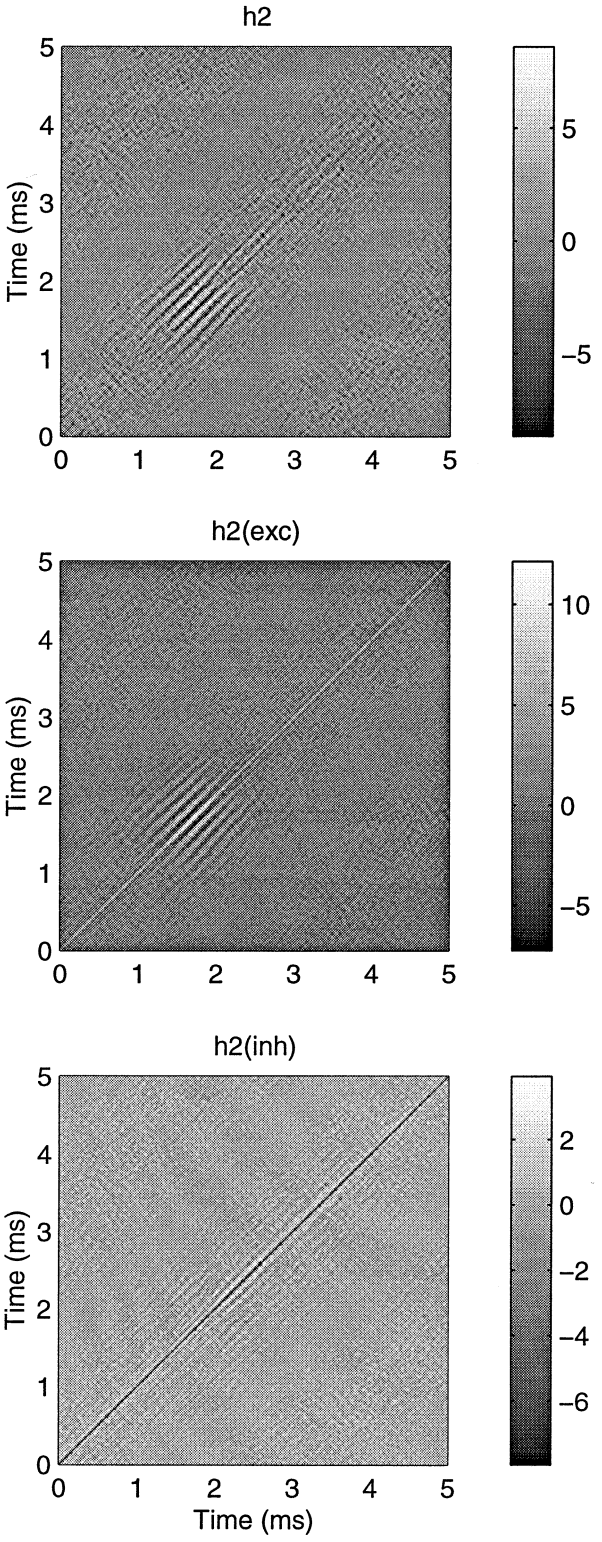

Fig. 13. Second-order Wiener kernel, with excitatory and inhibitory subkernels, for the axon of the second panel from the top in the right-hand column of Figs. 1, 2 and 5 (CF = 5.7 kHz). The patterns of parallel diagonal lines in these three panels are typical of high-frequency gerbil axons. They represent components in the PSTH that are phase-locked to the squares of the envelopes of filtered versions of the stimulus waveform.

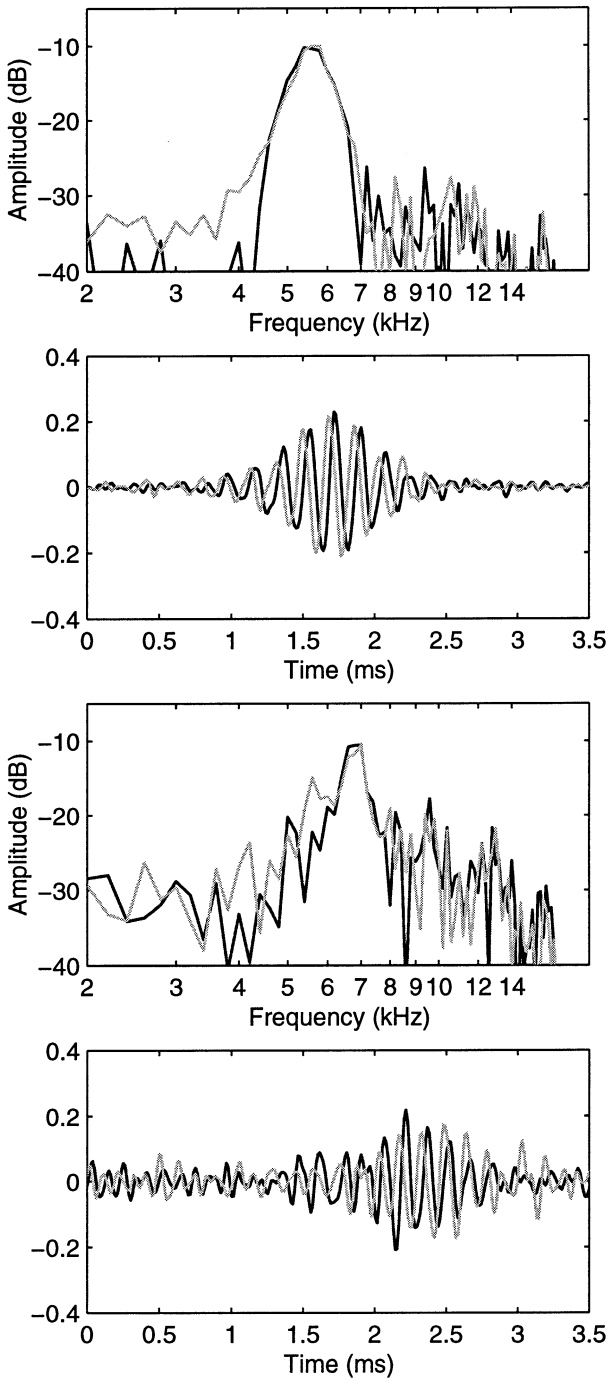

Fig. 14. The four highest-ranking eigenvectors (shown on a slightly expanded time scale) from the Wiener kernel of Fig. 13, along with the amplitude portions of their DFTs. The top two panels show the rank-1 eigenvector (black line) and the rank-2 eigenvector (gray line), both of which are excitatory (see Fig. 5, second from top panel, right-hand column). These two eigenvectors form a quadrature pair responsible in large measure for the pattern of parallel diagonal in h2exc of Fig. 13 (see Fig. 15). The bottom two panels show the rank-3 eigenvector (black line) and the rank-4 eigenvector (gray line), both of which are inhibitory. These two eigenvectors are responsible in large measure for the pattern of parallel diagonal lines between 2 and 3 ms in h2inh of Fig. 13 (see Fig. 16).

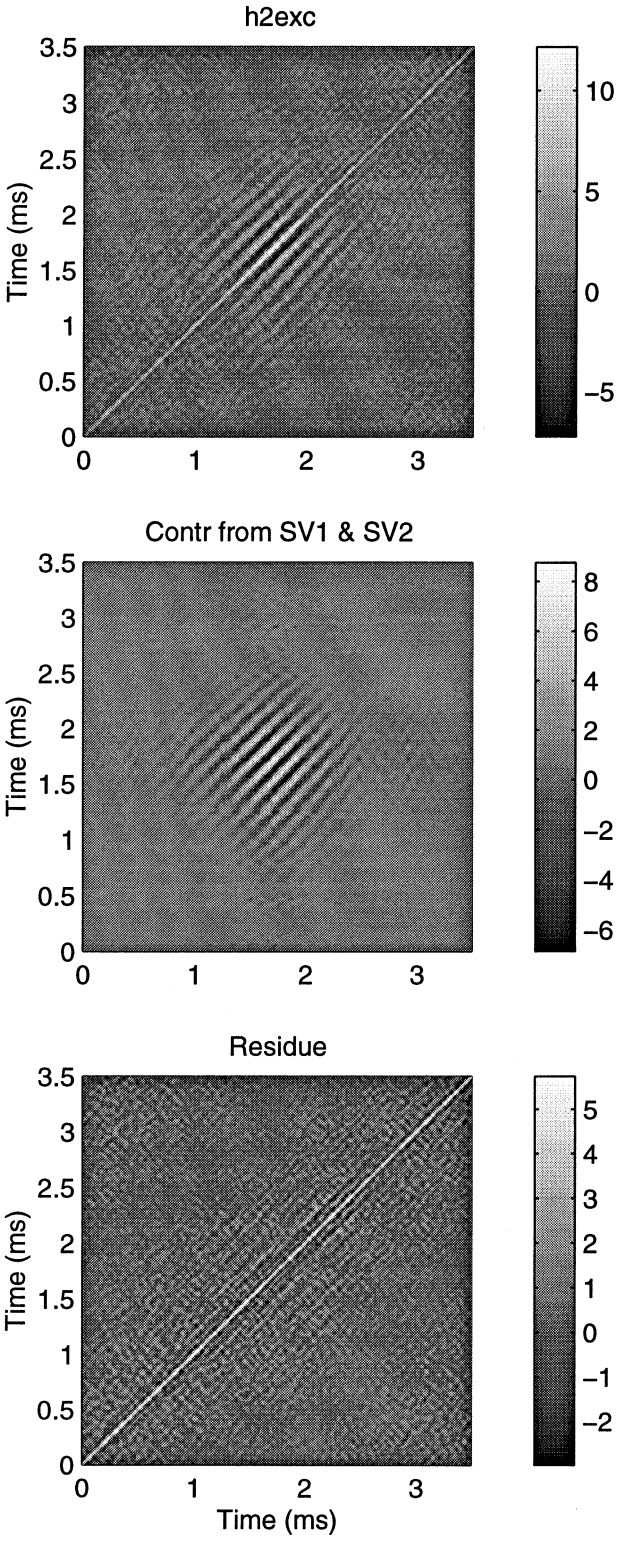

Fig. 15. Decomposition of the excitatory subkernel (h2exc) of Fig. 13. The middle panel shows the contribution from the quadrature pair of eigenvectors in the second panel of Fig. 14. The bottom panel shows the contribution from the remaining excitatory eigenvectors. The matrix (h2exc) in the top panel equals the sum of the other two matrices.

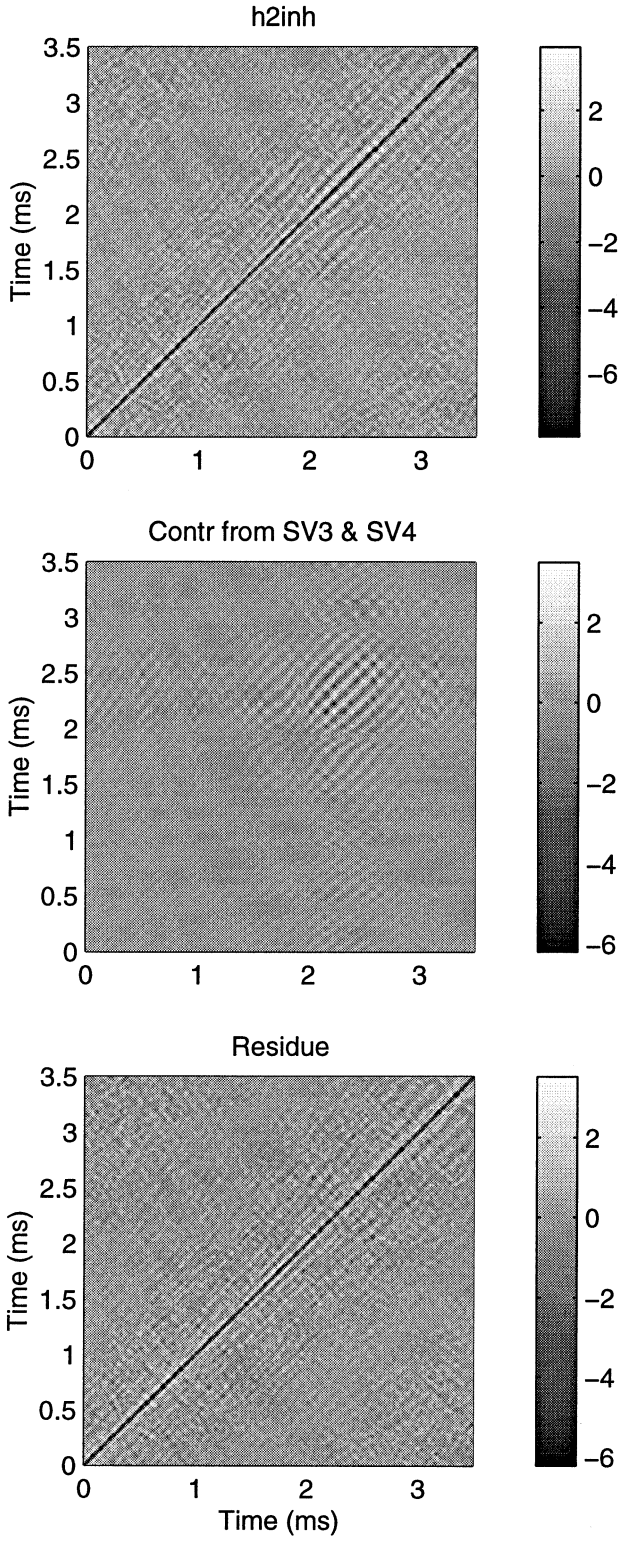

Fig. 16. Decomposition of the inhibitory subkernel (h2inh) of Fig. 13. The middle panel shows the contribution from the quadrature pair of eigenvectors in the bottom panel of Fig. 14. The bottom panel shows the contribution from the remaining inhibitory eigenvectors. The matrix (h2inh) in the top panel equals the sum of the other two matrices.

umns of Figs. 1, 2 and 5, only one (represented by the second from the top panel) exhibited a pair of eigenvectors with negative eigenvalues and rank higher than 5 (rank < 5). When this occurs, those eigenvectors typically exhibit conspicuous tuning and form a quadrature pair, and the second-order inhibitory subkernel typically has a corresponding, distinct patch of alternating dark and light, parallel diagonal lines. The eigenvectors and inhibitory subkernel in this case were not exceptions. Fig. 13 shows the second-order kernel and its subkernels, and Fig. 14 shows the four highest-ranking eigenvectors (and their DFTs) for this axon. The rank-1 and rank-2 eigenvectors, shown in the upper two panels of Fig. 14, have positive eigenvalues and therefore represent an excitatory process. Fig. 15 shows that they are almost entirely responsible for the patch of parallel diagonal lines in the excitatory subkernel. Together Figs. 14 and 15 imply that the predominant excitatory contribution of the second-order Wiener kernel to the predicted PSTH will be a spike rate increase that is phase-locked to the square of the envelope of the filtered stimulus waveform, the impulse response of the filter being either the rank-1 or rank-2 eigenvector (either waveform in the second panel of Fig. 14). They also imply that the spike rate at the present moment would exhibit such a component in response to a stimulus waveform that occurred between approximately 1.0 and 2.5 ms ago, and contained spectral energy in the vicinity of 6 kHz.

The quadrature pair formed by the rank-3 and rank-4 eigenvectors for this 6-kHz axon is shown in the bottom two panels of Fig. 14. The contribution of this pair of eigenvectors to the overall inhibitory subkernel for this axon is shown in Fig. 16. Clearly it accounts almost entirely for the small patch of parallel diagonal lines in the vicinity of 2 ms. Because these eigenvectors have negative eigenvalues, the contribution of the quadrature pair to the predicted PSTH will be a reduction of spike rate. The instantaneous amplitude of this reduction will be phase-locked to the square of the positive envelope of a filtered waveform; the filter's impulse response in this case will be either of the waveforms in the bottom panel of Fig. 14 (see Lewis et al., 2002). The spike rate at the present moment would exhibit such a component in response to a stimulus waveform that occurred between approximately 1.5 and 3 ms ago and contained spectral energy in the vicinity of 7 kHz. Fig. 17 shows the rank-1 and rank-3 eigenvectors with their amplitude DFTs plotted together. Owing to the spectral and temporal relationships of these two eigenvectors, we take the inhibitory (rank-3) eigenvector to represent the suppressive aspect of the phenomenon commonly called one- or two-tone suppression (see Section 5). The relative timing of the eigenvectors (and of the patches of diagonal lines in h_2(exc) and h_2(inh)) suggests that a

brief suppressive tone burst would be most effective if it were presented near the beginning of, or slightly ahead of the brief excitatory tone burst whose response it was intended to suppress. In the gerbil data sets we have analyzed so far, there are only nine axons (with CFs ranging approximately from 6 to 10 kHz) for which the patches of parallel diagonal lines in the inhibitory subkernels are sufficiently clean to allow this sort of judgement regarding relative timing. In all nine cases, one would draw the same conclusion that we did for this axon. A brief suppressive tone would be most effective if it were presented near the beginning (or slightly ahead) of the brief excitatory tone burst whose response it was intended to suppress.

4.4. PSTH prediction from a second-order Wiener kernel

The top panel in Fig. 18 shows the 400×400 excitatory subkernel for an axon with CF equal 6 kHz. The kernel was taken with a stimulus noise level of 22 dB SPL (for a 100-Hz bandwidth at 8 kHz). Notice that the patch of alternating dark and light parallel diagonal lines is faint in this case. Singular-value (or eigen) decomposition of the entire matrix yielded no conspicuously tuned eigenvectors. Therefore, we carried out the decomposition on the 151×151 submatrix that extended from 1.250 ms to 3.125 ms (covering the patch). The three highest-ranking eigenvectors from this decomposition were not tuned (see Appendix of Lewis et al., 2002, for discussion of extraction of filter functions from noisy second-order kernels). The rank-4 and rank-5 eigenvectors (SV4 and SV5) were tuned, however, and formed a quadrature pair (Fig. 19). The lower panel of Fig. 18 shows the contribution of these two eigenvectors to the original excitatory subkernel. This

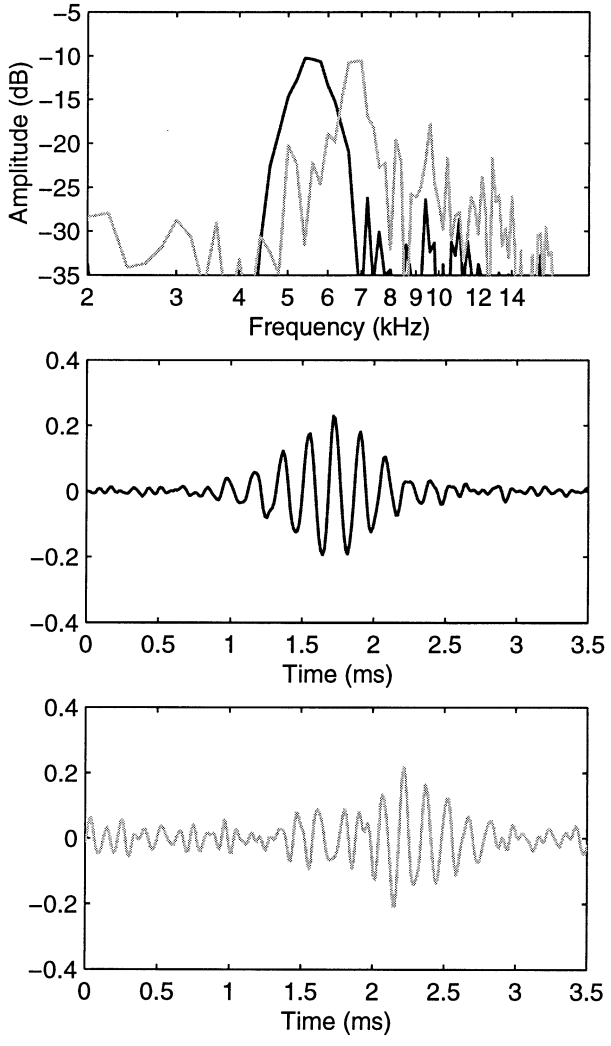

Fig. 17. Comparison of the rank-1 eigenvector (black line) and the rank-3 eigenvector (gray line) of Fig. 14.

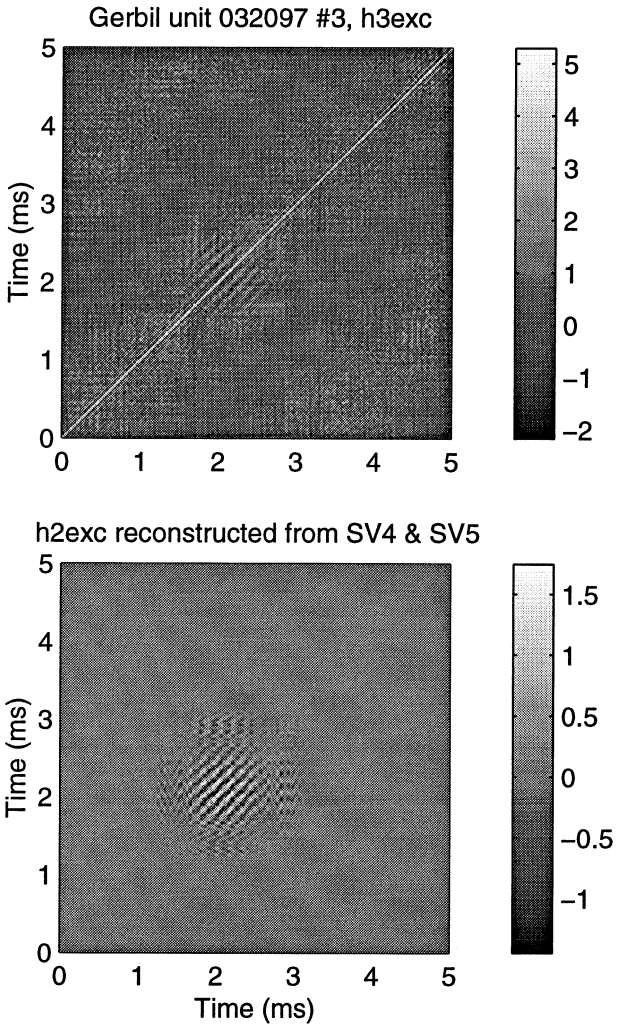

Fig. 18. Excitatory component (top panel) of the second-order Wiener kernel for an axon with CF close to 6 kHz. Although this kernel was unusually noisy, we were able to extract a well-tuned quadrature pair of eigenvectors (Fig. 19) that embodied the pattern of parallel diagonal lines (see text). The bottom panel shows the contribution of this quadrature pair to h2exc.

was constructed by embedding the 151-element eigenvectors, SV4 and SV5, in 400-element vectors, with the first 99 elements and the last 150 elements of each vector set equal to zero. The patch of parallel diagonal lines now stands out clearly.

Immediately before presentation of the continuing, nonrepeating noise stimulus for Wiener-kernel analysis, the stimulus waveform beginning at 5 ms in the lower panel of Fig. 20 had been presented approximately 2400 times. The first 5 ms of the waveform in Fig. 20 are a repetition of the last 5 ms. The noisy dark line in Fig. 21 was obtained by convolution of the complete stimulus waveform of Fig. 20 with the reduced excitatory subkernel in the lower panel of Fig. 18:

$$r_2(n) = \sum_{\tau=0}^{N-1}\sum_{\tau=0}^{N-1}\hat{h}_2(\tau_1,\tau_2)s(n-\tau_1)s(n-\tau_2) \qquad (3)$$

where $\hat{h}_2(\tau_1,\tau_2)$ was the reduced subkernel in the lower panel of Fig. 18; $s(\tau)$ was the entire waveform of Fig. 20; and $r_2(n)$ was the predicted contribution to the PSTH in response to that waveform, n being the histogram bin number. To avoid edge effects, the values of the predicted PSTH over the first 5 ms were discarded. The remainder covered the entire 74.35-ms duration of the stimulus. The observed PSTH, constructed from 27 159 spikes, recorded during the 2400 presentations of the stimulus waveform, is presented in gray in Fig. 21.

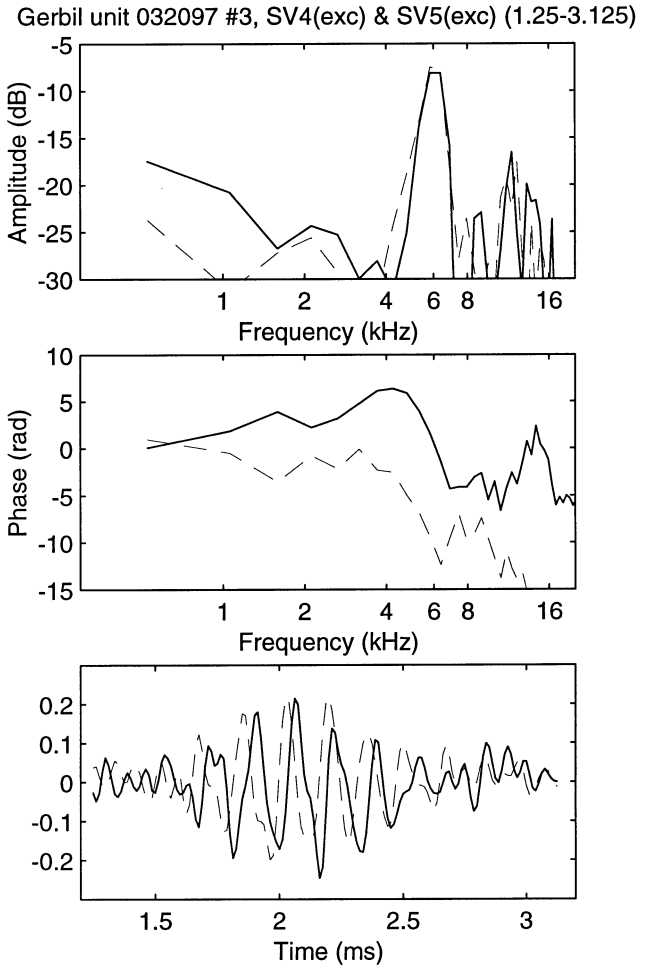

Fig. 19. The only well-tuned eigenvectors produced by singular-value decomposition of h2exc in Fig. 18.

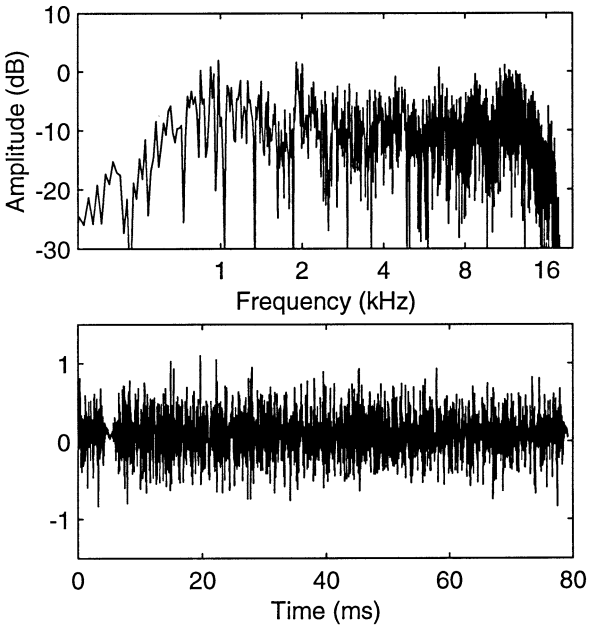

Fig. 20. Noise segment presented repeatedly as stimulus to the axon of Figs. 18 and 19. The stimulus waveform was recorded with a calibrated probe microphone (Etymotic ER-10B) sealed to the external ear canal. The lower panel shows slightly more than one full cycle of the stimulus. The upper trace shows the amplitude portion of its DFT.

5. Discussion

From one presentation of a repeated stimulus waveform to another, the pattern of spikes elicited in a given cochlear axon tends to vary markedly and, apparently, randomly. This may be a consequence, for example, of internal noise that provides a dithering effect (e.g., see Stein, 1970; Yu and Lewis, 1989; Lewis et al., 2000). As a result of the apparent randomness, when a PSTH is taken over a sufficiently large number of trials, it typically smooths over the effects of several phenomena, such as the finite duration of a spike (several tens of sampling intervals), refractoriness, and longer-term fluctuations in excitability that lead to spike clustering (e.g., see Teich et al., 1991; Edwards and Wakefield, 1993). In other words, the probability that, for a given axon, a spike will occur (i.e., be passing through its peak value

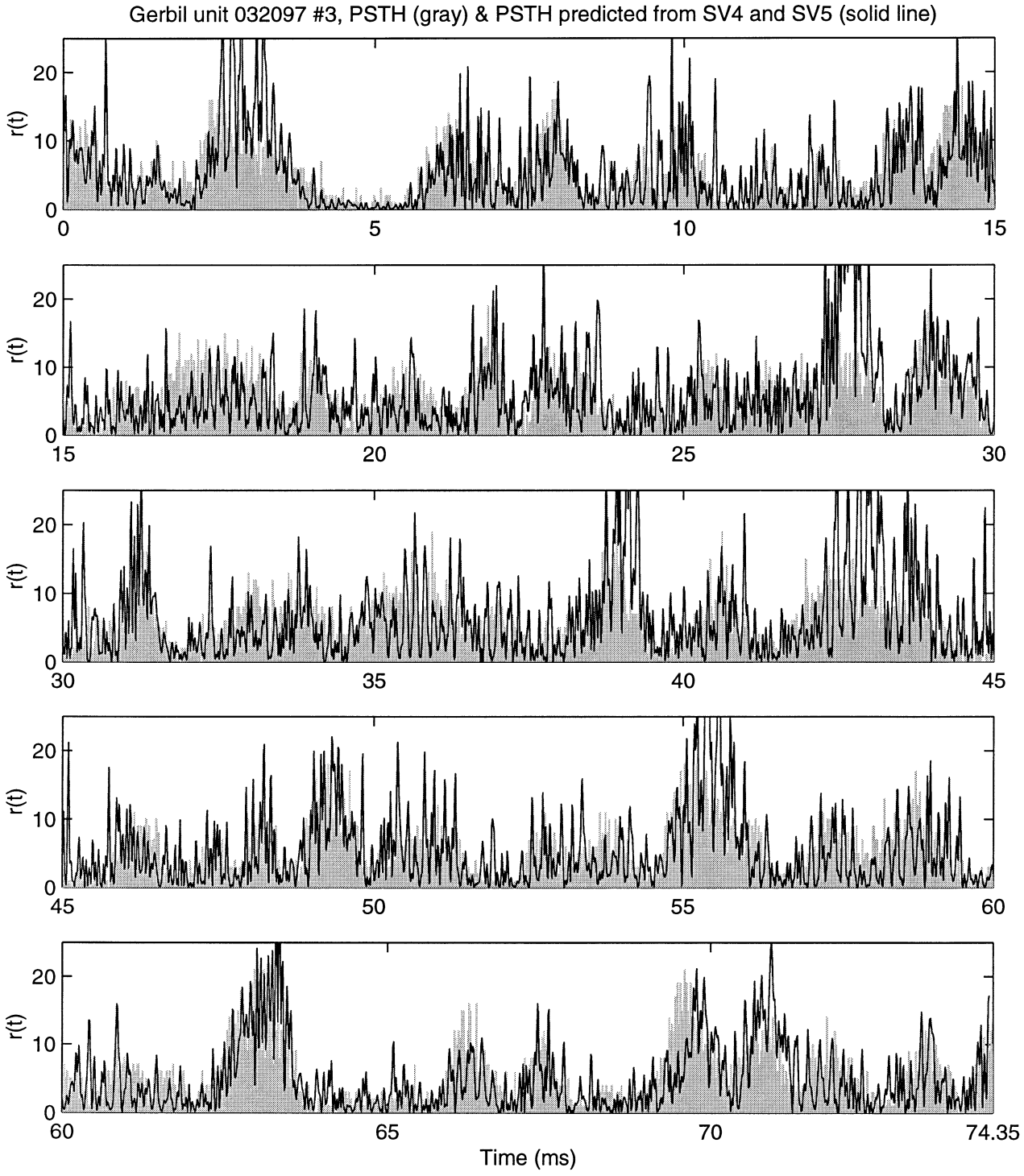

Fig. 21. PSTH (plotted in gray, constructed from 27 159 spikes) for the axon of Figs. 18 and 19 in response to approximately 2400 cycles of the stimulus of Fig. 20. The noisy dark line is the prediction of the PSTH by the filter functions of Fig. 19. The prediction was computed by convolution of the waveform in the lower panel of Fig. 20 with the reduced second-order kernel in the lower panel of Fig. 18.

– our criterion for occurrence) during a given moment (a given sampling interval) will depend on factors other than the recent history of the stimulus (e.g., it will depend on precisely when the previous spike occurred). The typical PSTH gives us an averaged probability, one that does not include those factors. To the extent that Wiener kernels predict the PSTH, it is this averaged probability that they are predicting, moment by moment through the presentation of the stimulus waveform.

The quality of the prediction in Fig. 21 suffers from the noisiness apparent in the waveforms (eigenvectors) in the bottom panel of Fig. 19, which were used to make the prediction. A perfectly matched quadrature pair of eigenvectors generates a prediction that smoothly follows the square of the envelope of the filtered waveform. This is easily seen in simulations with quadrature gammatone functions (see Lewis et al., 2002). When we have added even small amounts of noise to these functions, taking them out of perfect quadrature matching, the predictions are contaminated with components that correspond to a distorted version of the filtered waveform itself (as opposed to the square of its envelope). Owing to that contamination, we did not address the goodness of fit in a quantitative way (e.g., Eggermont et al., 1983a,b); we plan to address that issue in a subsequent paper. Regarding the presence of eigenvectors in quadrature pairs, one should keep in mind that this is an arbitrary mathematical decomposition of a pattern (diagonal parallel lines) in the second-order Wiener kernel. The pattern itself represents a process that produces an output waveform equal to the square of the envelope of a linearly filtered version of the input waveform.

In the chinchilla, Recio et al. (1997) found no significant patterns in the second-order Wiener kernels taken for basilar membrane motion in response to white noise auditory stimulus applied to the external ear canal. If this were true for the gerbil as well, then the nonlinearities that gave rise to the patterns that we observed must occur in the signal path after the basilar membrane (between the basilar membrane and the spike trigger of the primary afferent axon). The nonlinear transduction process of the inner hair cell (Hudspeth and Corey, 1977) seems a likely candidate. On the other hand, at the level of the basilar membrane in the squirrel monkey, Rhode (1976) found that the amplitude of the response to one tone was reduced by the presence of a second, higher tone. This suggests that the effects of the phenomenon commonly called two-tone suppression involve reduction in ac gain and occur earlier in the signal path. A reduction in ac gain would not be apparent in the patterns of a second-order Wiener kernel (see Lewis et al., 2002). The suppressive effects that we observed, in the patterns of the second-order Wiener kernel, corresponded to negative shifts in dc spike rate. We found them in approximately one in five high-CF axons. This is approximately the proportion of gerbil high-CF axons in which we previously had observed one-tone suppression (Henry and Lewis, 1992). The effects of one-tone suppression include conspicuous negative shifts in dc spike rate (e.g., see figure 15 in Lewis and Henry, 1989). In the frog amphibian papilla, suppression seems consistently to involve negative shifts in dc spike rate (Lewis et al., 2002; see also Lewis, 1986).

For this form of suppression (negative shift in the short-term dc spike rate), our conclusion regarding the most effective timing of a brief high-side suppressor stimulus for the gerbil cochlea contrasts with that for the frog amphibian papilla. In the gerbil case ($n = 9$ axons), the inhibitory subkernels imply that a brief (e.g., 1-ms) high-side suppressor tone burst would be most effective if it were presented early in, or slightly (e.g., 0.5 ms) ahead of the presentation of a brief tone burst whose response it is intended to suppress. The inhibitory subkernels for the frog ($n = $ many) implied that a high-side suppressor burst would be most effective if applied late in the presentation of the other burst (Lewis et al., 2002). In both animals the suppressive pattern in the inhibitory subkernel implied that the presence of the excitatory stimulus was unnecessary for the production of the suppressive response (the negative shift in dc spike rate).

Acknowledgements

The research reported here was supported by the National Institute of Deafness and Communicative Disorders (Grant DC-00112). We thank Eva Hecht for assistance.

References

Carney, L.H., Yin, C.T., 1988. Temporal coding of resonances by low-frequency auditory nerve fibers: single-fiber responses and a population model. J. Neuropysiol. 60, 1653–1677.

de Boer, E., de Jongh, H.R., 1978. On cochlear encoding: potentialities and limitations of the reverse-correlation technique. J. Acoust. Soc. Am. 63, 115–135.

de Boer, E., Kuyper, P., 1968. Triggered correlation. IEEE Trans. Biomed. Eng. 15, 169–179.

Edwards, B.W., Wakefield, G.H., 1993. The spectral shaping of neural discharges by refractory effects. J. Acoust. Soc. Am. 93, 3353–3364.

Eggermont, J.J., 1993. Wiener and Volterra analyses applied to the auditory system. Hear. Res. 66, 177–201.

Eggermont, J.J., Aertsen, A.M.H.J., Johannesma, P.I.M., 1983a. Quantitative characterisation procedure for auditory neurons based on the spectro-temporal receptive field. Hear. Res. 10, 167–190.

Eggermont, J.J., Aertsen, A.M.H.J., Johannesma, P.I.M., 1983b. Prediction of the responses of auditory neurons in the midbrain of the grass frog based on the spectro-temporal receptive field. Hear. Res. 10, 191–202.

Eggermont, J.J., Johannesma, P.I.M., Aertsen, A.M.H.J., 1983c. Reverse-correlation methods in auditory research. Q. Rev. Biophys. 16, 341–414.

Evans, E.F., 1977. Frequency selectivity at high-signal levels of single units in cochlear nerve and nucleus. In: Evans, E.F., Wilson, J.P. (Eds.), Psychophysics and Physiology of Hearing. Academic Press, London, pp. 185–196.

Evans, E.F., 1989. Cochlear filtering: a view seen through the temporal discharge patterns of single cochlear nerve fibers. In: Wilson

J.P., Kemp D.T. (Eds.), Cochlear Mechanisms, Structure, Function and Models. Plenum, New York, pp. 241–250.
Henry, K.R., Lewis, E.R., 1992. One-tone suppression in the cochlear nerve of the gerbil. Hear. Res. 63, 1–6.
Hudspeth, A.J., Corey, D.P., 1977. Sensitivity, polarity, and conductance changes in the response of vertebrate hair cells to controlled mechanical stimuli. Proc. Natl. Acad. Sci. USA 74, 2407–2411.
Lewis, E.R., 1986. Adaptation, suppression and tuning in amphibian acoustical fibers. In: Moore, B.C.J., Patterson, R.D. (Eds.), Auditory Frequency Analysis. Plenum, New York, pp. 129–136.
Lewis, E.R., Henry, K.R., 1989. Transient responses to tone bursts. Hear. Res. 37, 219–240.
Lewis, E.R., Henry, K.R., 1994. Dynamic changes in tuning in the gerbil cochlea. Hear. Res. 79, 183–189.
Lewis, E.R., Henry, K.R., 1995. Nonlinear effects of noise on phase-locked cochlear nerve responses to sinusoidal stimuli. Hear. Res. 92, 1–16.
Lewis, E.R., Henry, K.R., Yamada, W.M., 2000. Essential roles of noise in neural coding and in studies of neural coding. Biosystems 58, 109–115.
Lewis, E.R., Henry, K.R., Yamada, W.M., 2002. Tuning and timing of excitation and inhibition in primary auditory nerve fibers. Hear. Res. 171, 13–31.
Møller, A.R., 1986. Systems identification using pseudorandom noise applied to a sensorineural system. Comp. Math. Appl. 12A, 803–814.
Recio, A., Narayan, S.S., Ruggero, M.A., 1997. Wiener-kernel analysis of basilar-membrane responses to white noise. In: Lewis, E.R., Long, G.R., Lyon, R.F., Narins, P.M., Steele, C.R., Hecht-Poinar, E. (Eds.), Diversity in Auditory Mechanics. World Scientific Press, Singapore, pp. 325–331.
Rhode, W.S., 1976. Some observations on two-tone interactions measured by the Mossbauer effect. In: Evans, E.F. and Wilson, J.P. (Eds.), Psychophysics and Physiology of Hearing. Academic Press, New York, pp. 27–38.
Stein, R.B., 1970. The role of spike trains in transmitting and distorting sensory signals. In: Schmidt, F.O. (Ed.), The Neurosciences. Rockefeller University Press, New York, pp. 597–604.
Teich, M.C., Turcott, R.G., Lowen, S.B., 1991. The fractal doubly stochastic Poisson point process as a model for cochlear neural spike train. In: Dallos, P., Geisler, C.D., Matthews, J.W., Ruggero, M.A., Steele, C.R. (Eds.), Mechanics and Biophysics of Hearing. Plenum, New York, pp. 354–361.
van Dijk, P., Wit, H.P., Segenhout, J.M., Tubis, A., 1994. Wiener kernel analysis of inner-ear function in the American bullfrog. J. Acoust. Soc. Am. 95, 904–919.
van Dijk, P., Wit, H.P., Segenhout, J.M., 1997a. Dissecting the frog inner ear with Gaussian noise. I. Application of high-order Wiener-kernel analysis. Hear. Res. 114, 229–242.
van Dijk, P., Wit, H.P., Segenhout, J.M., 1997b. Dissecting the frog inner ear with Gaussian noise. II. Temperature-dependence of inner-ear function. Hear. Res. 114, 243–251.
Wolodkin, G., Yamada, W.M., Lewis, E.R., Henry, K.R., 1997. Spike rate models for auditory nerve fibers. In: Lewis, E.R., Long, G.R., Lyon, R.F., Narins, P.M., Steele, C.R., Hecht-Poinar, E. (Eds.), Diversity in Auditory Mechanics. World Scientific Press, Singapore, pp. 104–110.
Yamada, W.M., 1997. Second-order Wiener Kernel Analysis of Auditory Afferent Axons of the North American Bullfrog and Mongolian Gerbil Responding to Noise. Doctoral dissertation, Graduate Group in Neurobiology, University of California, Berkeley, CA.
Yamada, W.M., Lewis, E.R., 1999. Predicting the temporal responses of non-phase-locking bullfrog auditory units to complex acoustic waveforms. Hear. Res. 130, 155–170.
Yu, X., Lewis, E.R., 1989. Studies with spike initiators: linearization by noise allows continuous signal modulation in neural networks. IEEE Trans. Biomed. Eng. 36, 36–43.